INSTITUT FRANCO-ALLEMAND DE RECHERCHES DE SAINT-LOUIS
DEUTSCH-FRANZÖSISCHES FORSCHUNGSINSTITUT SAINT-LOUIS

5 rue du Général Cassagnou - 68301 SAINT-LOUIS
Tél. +33 (0)3 89 69 50 00 - Fax +33 (0)3 89 69 50 00
Adresse postale : F-68301 SAINT-LOUIS CEDEX - BP 34
Postanschrift: Postfach 1260 - D 79574 WEIL AM RHEIN

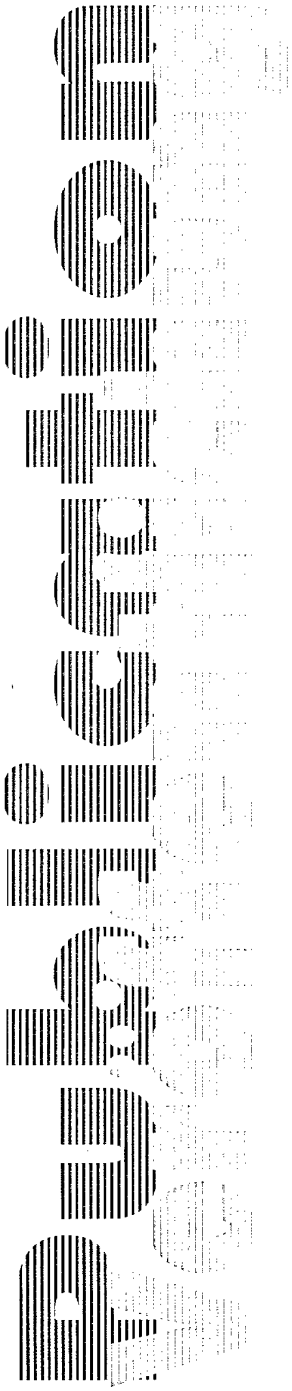

Enhanced Doppler Picture Velocimetry (DPV) for Planar Velocity Measurements in High-Speed Tunnel Flow

SEILER F., GEORGE A., LEOPOLD F.,
HAVERMANN M., SRULIJES J.

ISFV10
10th International Symposium on Flow Visualization
Kyoto, Japan, August 26-29, 2002

PU 621/2002

Axe de recherches
Schwerpunkt 2.14

REPORT DOCUMENTATION PAGE

Form Approved OMB No. 0704-0188

1. AGENCY USE ONLY (Leave blank)	2. REPORT DATE	3. REPORT TYPE AND DATES COVERED
	2002	Symposium report, 26-29 August 2002

4. TITLE AND SUBTITLE

Enhanced Doppler Picture Velocimetry (DPV) for Planar Velocity Measurements in High Speed Shock Tunnel Flow

5. FUNDING NUMBERS

6. AUTHOR(S)

F. Seiler, A. George, F. Leopold, M. Havermann, J. Srulijes

7. PERFORMING ORGANIZATION NAME(S) AND ADDRESS(ES)

Institut franco-allemand de recherches de Saint-Louis (ISL)
5 rue du General Cassagnou, F-68301 Saint-Louis, France

8. PERFORMING ORGANIZATION REPORT NUMBER

9. SPONSORING/MONITORING AGENCY NAME(S) AND ADDRESS(ES

Institut franco-allemand de recherches de Saint-Louis (ISL)
5 rue du General Cassagnou, F-68301 Saint-Louis, France

10. SPONSORING/MONITORING AGENCY REPORT NUMBER

PU 621/2002

11. SUPPLEMENTARY NOTES

Text in English, 26 figures (some color plates), 13 references, 13 pages. 10th International Symposium on Flow Visualization, Kyoto, Japan, August 26-29 2002.

12a. DISTRIBUTION/AVAILABILITY STATEMENT

Distribution authorized to U.S. Department of Defense (DoD) components only; Foreign Government Information. 12 November 2002. Other requests for this document shall be referred to Embassy of Germany, 4645 Reservoir Road, NW, Washington DC 20007-1998. "These documents may be passed without express permission of the German Ministry of Defense – Rue VII 6 – only to German Federal Armed Forces Agencies or military of other NATO States."

12b. DISTRIBUTION CODE

ABSTRACT (Maximum 200 words)

A technique for visualizing a velocity field in an entire plane has been developed by taking so-called "Doppler Pictures" using Michelson interferometry. With the Doppler Picture Velocimetry (DPV) information about the instantaneous and local velocities of tracers passing through a light sheet are available. The tracer particles are illuminated by a laser light source and the frequency of the scattered light, in case of moving particles, is shifted by the Doppler effect. This small Doppler shift of the frequency of the light scattered by tracer particles is transformed by a Michelson interferometer into varying light intensities as interferometer output. Therefore, the light intensity distribution on the Doppler picture gives information on the Doppler frequency shift and in consequence on the speed of the tracer particles crossing the light sheet plane. The technique for taking and processing the Doppler picture images was enhanced in the last years and the status of progress of the DPV method will be described first with the tests using a rotating disc and a free jet for DPV technique calibration, and secondly with an application in high speed fluid mechanics showing the velocity distribution in a light sheet plane crossing a supersonic wedge flow generated in ISL's high energy shock tunnel STB. The Doppler picture, taken with the enhanced set-up by a CCD camera, is pixel-wise computer-processed for velocity presentation using an image processing software which is specially developed at ISL for DPV purposes.

14. SUBJECT TERMS

ISL, German, Light sheet, Tracer, Velocity visualization, Michelson interferometer, Doppler picture

15. NUMBER OF PAGES

16. PRICE CODE

17. SECURITY CLASSIFICATION OF REPORT	18. SECURITY CLASSIFICATION OF THIS PAGE	19. SECURITY CLASSIFICATION OF ABSTRACT	20. LIMITATION OF ABSTRACT
UNCLASSIFIED	UNCLASSIFIED	UNCLASSIFIED	UL

Enhanced Doppler Picture Velocimetry (DPV) for Planar Velocity Measurements in High Speed Shock Tunnel Flow

F. Seiler, A. George, F. Leopold, M. Havermann, J. Srulijes

French-German Research Institute of Saint-Louis (ISL)
5, Rue du Général Cassagnou, F-68301 Saint-Louis, France
Tel: +33 3 8969 5042 / Fax: +33 3 8969 5048 / e-mail: seiler@isl.tm.fr

Abstract: A technique for visualizing a velocity field in an entire plane has been developed by taking so-called "Doppler Pictures" using Michelson interferometry. With the Doppler Picture Velocimetry (DPV) information about the instantaneous and local velocities of tracers passing through a light sheet are available. The tracer particles are illuminated by a laser light source and the frequency of the scattered light, in case of moving particles, is shifted by the Doppler effect. This small Doppler shift of the frequency of the light scattered by tracer particles is transformed by a Michelson interferometer into varying light intensities as interferometer output. Therefore, the light intensity distribution on the Doppler picture gives information on the Doppler frequency shift and in consequence on the speed of the tracer particles crossing the light sheet plane. The technique for taking and processing the Doppler picture images was enhanced in the last years and the status of progress of the DPV method will be described first with the tests using a rotating disc and a free jet for DPV technique calibration, and secondly with an application in high speed fluid mechanics showing the velocity distribution in a light sheet plane crossing a supersonic wedge flow generated in ISL's high energy shock tunnel STB. The Doppler picture, taken with the enhanced set-up by a CCD camera, is pixel-wise computer-processed for velocity presentation using an image processing software which is specially developed at ISL for DPV purposes.

Keywords: Light sheet, Tracer, Velocity visualization, Michelson interferometer, Doppler picture

1. Introduction

Some measuring techniques have been developed for taking a picture of the velocity distribution, for example in a light sheet crossing a gas flow. A well-known technique is the Particle Image Velocimetry (PIV), which is an often used tool for this purpose (Merzkirch, 1990). Also Doppler Global Velocimetry (DGV) is known, using an amplitude light filter for analysing the Doppler shift of the frequency of the light scattered by tracer particles (Meyers, 1992). At ISL a special Michelson interferometer was designed (Oertel et al., 1981) to transform the Doppler frequency shift of the light scattered by tracer particles passing a light sheet into a shift of the light intensity leaving the interferometer. The changes in the light intensity distribution can be directly related to the velocities of the tracer particles. This method, called Doppler Picture Velocimetry (DPV), was further developed during the last years (Seiler et al. ,1987, 1991, 1998) and the actual status of the DPV set-up and the technique for processing the interference image of the Doppler picture will be described herein. Some details on the progress in image processing were already described by Seiler et al. (1999) and Leopold et al. (2000).

2. Principles of DPV technique

2.1 Doppler effect

In order to measure the tracer velocity $\vec{v}$, the well-known relation of single-beam velocimetry is used as given in Equation (1) with the unit vectors $\vec{e}_L$ and $\vec{e}_D$. In Figure 1 the vector $\vec{e}_L$ denotes the direction of illumination by the light source (L), and the vector $\vec{e}_D$ is directed from the tracers to the Michelson interferometer detector (D). θ is the angle between the two unit vectors $\vec{e}_L$ and $\vec{e}_D$. The velocity component of the flow vector $\vec{v}$ is

measured in the direction of the difference vector $\vec{e}_D - \vec{e}_L$ which forms the angle γ to the velocity vector $\vec{v}$, as shown in Figure 1. The Doppler frequency shift can be deduced with the Doppler effect relations as follows:

$$\frac{dv_L}{v_L} = \frac{\vec{v}\,(\vec{e}_D - \vec{e}_L)}{c} = 2\frac{v}{c}\cos\gamma \sin\frac{\theta}{2}. \qquad (1)$$

The laser light source frequency is denoted by v_L. By Doppler effect that frequency is shifted to v_D and the Doppler shift $dv_L = v_D - v_L$ is analyzed via the Michelson interferometer.

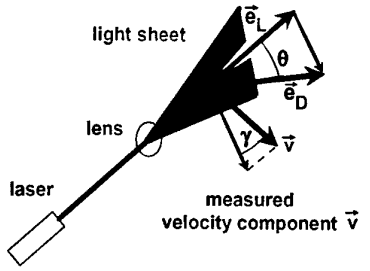

Fig. 1 Doppler effect

2.2 *Michelson interferometer*

A plane Σ crossing the gas flow is illuminated by a light sheet with frequency v_L. In order to visualise the velocity distribution in this plane Σ, tracer particles are seeded into the flow and the light scattered from these particles is focused into a specially designed Michelson interferometer (Seiler and Oertel, 1983), see Figure 2.

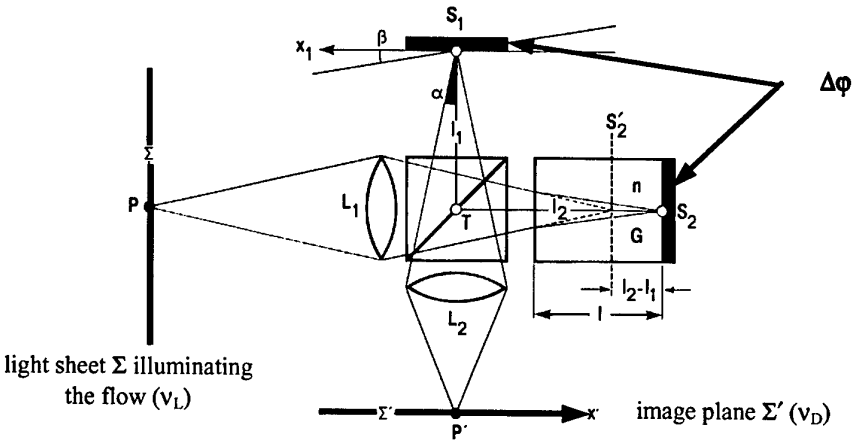

Fig. 2 Whole field Michelson interferometer

The Michelson interferometer in Figure 2 consists of a beam splitter cube T with a 50% reflecting mirror, the two mirrors S_1 and S_2 and the glass block G between S_2 and T. The scattered light coming from the object plane Σ and passing through the lens L_1 is divided by the beam splitter T into two parts of equal intensity. These two parts are focussed by the lens L_1 on S_1 and S_2, respectively. With the lens L_2 the image of the object plane Σ on S_1 and S_2 is transferred to the image plane Σ'. The Michelson interferometer works as a spectrometer for detecting the Doppler shift of the frequency of the light scattered by tracer particles and its mechanism is described in the following. In the image plane Σ' the light coming from the two interferometer legs (1) and (2) interferes and the light intensity I at all image points P' in Σ', as a result of that interference, depends on the phase difference $\Delta\varphi$, see Figure 2, originated in the two legs of the Michelson interferometer as given in the following relation, with I the light intensity occurring by light interference on the image plane Σ', and I_0 the light intensity as it is scattered by the tracer particles:

$$I = I_0 \cos^2\frac{\Delta\varphi}{2}\,, \text{ normalized relation: } \frac{I}{I_0} = \cos^2\frac{\Delta\varphi}{2} \text{ with } 0 \le \frac{I}{I_0} \le 1\,. \qquad (2)$$

The phase difference $\Delta\varphi$ is a function of three quantities: the optical path difference $\Delta\phi$, with

$$\Delta\phi = 2n\left|l_2 - l_1\right|, \qquad (3)$$

the light source frequency v_L and the speed of light c_0 in vacuum, as follows:

$$\frac{\Delta\varphi}{2\pi}=\nu_L\,\frac{\Delta\phi}{c_0}\,. \tag{4}$$

In differentiating $\Delta\varphi$ in Equation (4) to $d\nu_L$, the expression (5) is obtained. Equation (5) explains that frequency changes $d\nu_L$, due to the Doppler effect, are directly proportional to variations $d(\Delta\varphi)$ of the phase difference $\Delta\varphi$.

$$d\left(\frac{\Delta\varphi}{2\pi}\right)=\frac{\Delta\phi}{c_0}\,d\nu_L\,. \tag{5}$$

The light scattered from the light sheet plane Σ is Doppler shifted to ν_D in the case of tracer displacement caused by flow movement. The frequency changes

$$d\nu_L=\nu_D-\nu_L\,. \tag{6}$$

of the scattered light coming from the plane Σ are transformed into changes $d(\Delta\varphi)$, see Equation (5), of the phase difference $\Delta\varphi$ between the two legs of the Michelson interferometer. As already said, in Equations (1), (4), (5) and (6) the index (L) denotes the light source, index (D) the detector, i.e., the Michelson interferometer. The $d(\Delta\varphi)$ change in Equation (5) causes variations dI of the interference light intensity I in the plane Σ', as:

$$dI=-\frac{I_0}{2}\sin\Delta\varphi\cdot d(\Delta\varphi)\,. \tag{7}$$

Therefore, the light intensity distribution I in Σ' (Doppler picture), relative to the initially adjusted I as reference image, informs on the frequency shift $d\nu_L$ which is proportional to the tracer speed: relation see Equation (1). I.e., at all points P' in Σ' dI is given as: dI = I (reference image) – I (Doppler picture).

The Michelson interferometer is adjusted initially, before flow onset, to interference fringes by turning the mirror S_I by a small angle β as depicted in Figure 2. It would be preferable to adjust the interferometer to a homogeneously light intensity output, which is a constantly distributed light intensity I in plane Σ', but is not recommendable in practice because the optical components such as mirrors, lenses and other parts used have only a limited optical accuracy. Therefore, the best alternative is to adjust the Michelson interferometer initially to the easily obtainable interference fringe pattern mentioned (Seiler and George, 1986).

3. Tests for DPV system calibration

3.1 Rotating disc

The periphery of a rotating disc is illuminated by a 1 W Ar^+-laser from a direction nearly perpendicular to the axis of rotation. The scattered light is observed in the back scattered direction, see principle sketch in Figure. 3.

For the rotating disc, the velocity vector of the "scattering surface" is tangential to the surface. This tangential velocity can be divided in two vectors: one vector in the direction of observation (Michelson interferometer) and one perpendicularly to that, which causes no Doppler effect.

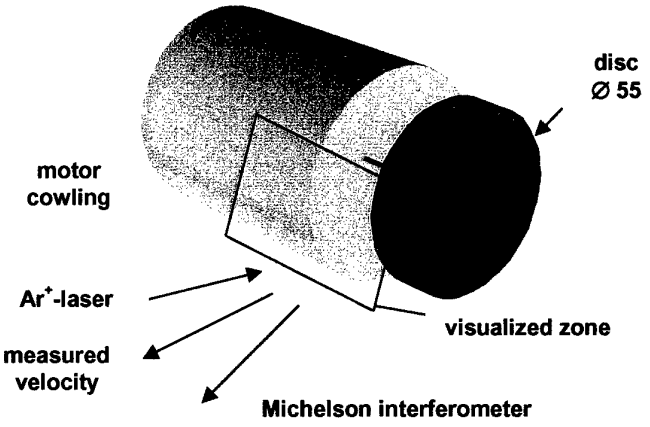

Fig. 3 Set-up of the rotating disc

The measured velocity component $\vec{v}$ is, according to Equation (1), proportional to the Doppler shift $d\nu_L=\nu_D-\nu_L$ which is processed by the Michelson interferometer for velocity determination.

In the Doppler picture technique, the interference fringes have been adjusted by turning the mirror S_1 by a small angle β, see optical-set-up in Figure 2. Then straight and parallel interference fringes appear, see Figure 4a. Two fringe light intensity patterns are visible which depend on the phase difference $\Delta\varphi$ according to the $\cos^2$-distribution in Equation (2). On the left hand side of the Doppler picture in Figure 4a the interference fringe system is formed by the light scattered from the motor cowling at rest, and on the right the fringe system comes from the light scattered from the rotating disc periphery. The disc axis is at the top of Figure 4a.

In order to evaluate the velocity at each pixel of the CCD camera, at first each of the two interference fringe systems is normalized with the actual light intensity distribution I_0 (Figure 4b), with I/I_0 according to Equation (2). I_0 is captured by the camera CCD1, see Figure 5. Imperfections in the optical parts, non-uniformity of pixel distribution and disorientations make the exact overlay of the interference (CCD2) and intensity images (CCD1) very difficult (Meyers 1992).

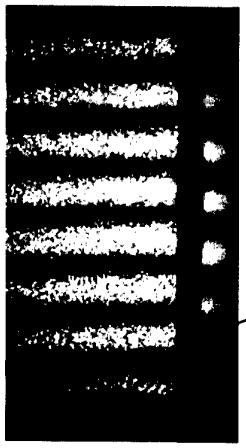

Fig. 4a CCD2 interference image

Therefore, after each alignment of the optical system, several images of the calibration card placed in the light sheet plane are recorded. The calibration card consists of 4 different lines and 36 grid points, Figure 6. The 4 lines were detected with an algorithm developed at ISL by Schneider (1987). By means of the information concerning the position and the orientation of these lines, the images can be correctly aligned to each other.

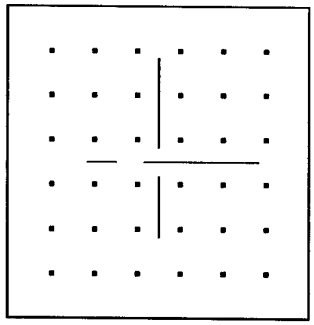

Fig. 6 Calibration card

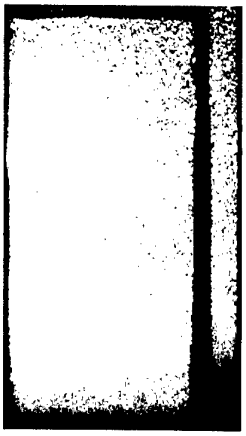

Fig. 4b CCD1 image

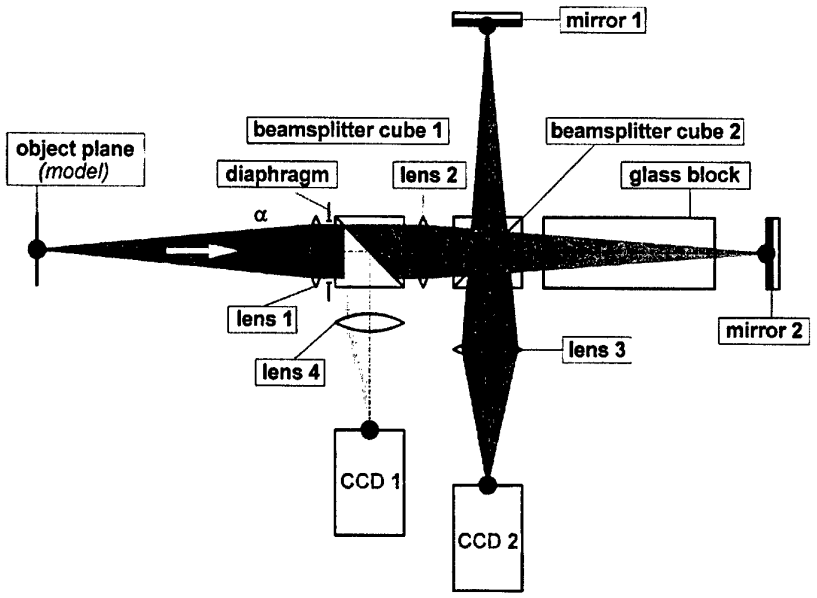

Fig. 5 Intensity camera CCD1 and DPV camera CCD2

Several sets of linear equations are established in order to move the grid points of the calibration card from their imaged to their overlayed positions. To get an accurate transformation of the gray values, the interpolation technique described by Schumacher (1996) is applied.

Because of contrast variations in the DPV pictures, Equation (2) is not really fulfilled with $0 \le I/I_0 \le 1$ over the whole interference fringe picture, i.e., the maximum gray values as well as the minimum values fluctuate. The largest G_{max} and smallest G_{mim} gray values are determined with every pixel on the CCD chip in its (x, y)-plane and a second normalization technique is applied, using the G_{min} and G_{max} values in the following way:

$$G(x,y) = G_{min} + (G_{max} - G_{min})\cos^2\left(\frac{\Delta\varphi}{2}\right). \tag{8}$$

In using the expression

$$I(x,y) = \frac{G(x,y) - G_{min}}{G_{max} - G_{min}} = \cos^2\frac{\Delta\varphi}{2}, \tag{9}$$

the equation (9) is transformed to $\Delta\varphi$ which results, in case of motionless motor cowling as reference, to:

$$\Delta\varphi_L = \arccos\left(2I(x,y)_L - 1\right) \pm n \qquad n = 1,2,3,... \tag{10}$$

$I(x, y)_L$ is determined from Figure 4a, left hand side disc fringe pattern. The periodical fringe pattern cause an increase of n. For the right hand side of the interference fringe distribution, $\Delta\varphi$ is determined in the same way:

$$\Delta\varphi_D = \arccos\left(2I(x,y)_D - 1\right) \pm n \qquad n = 1,2,3,... \tag{11}$$

Finally, assuming a small difference between the laser frequency ν_L and the Doppler shifted one ν_D, the Doppler shift $d\nu_L$ results from Equation (5) as:

$$d\nu_L = \frac{c_0}{\Delta\phi} d\left(\frac{\Delta\varphi}{2\pi}\right), \tag{12a}$$

with

$$d(\Delta\varphi) = \Delta\varphi_D - \Delta\varphi_L \tag{12b}$$

Figure 7 shows the Doppler picture in terms of the phase difference $\Delta\varphi$ treated as described by Equation (10) and Equation (11) as pseudo color distribution. Figure 8 represents the velocities measured at each pixel of the Doppler picture image applying Equation (1) and Equations (12a,b). The disc axis is located at x = 23 mm at zero speed measured. There are small differences between theory and Doppler picture measurement which increase towards the upper part of the disc for $x \rightarrow 0$. The deviation is systematic and probably caused by the inaccuracy of the calculated speed distribution (≈5%) and by the error of Doppler picture processing (maximum error of is 10%), which increase with the decreasing fringe contrast towards $x \rightarrow 0$.

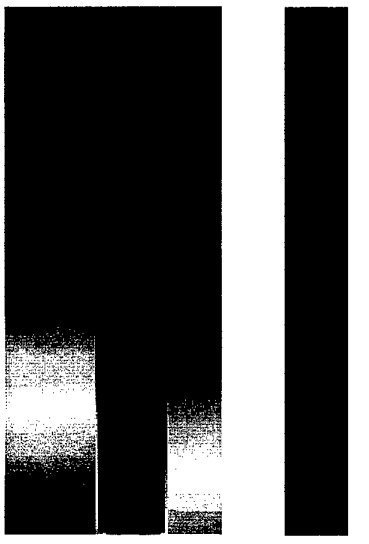

Fig. 7 Pseudo color Doppler pictures
(left: motionless, right: rotating disc)

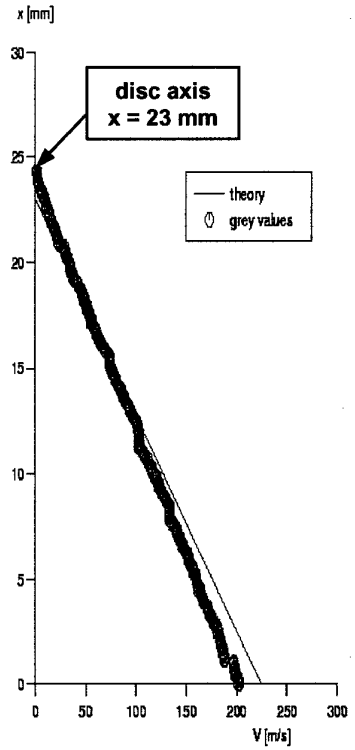

Fig. 8 Velocity distribution

3.2 Free jet flow

Figure 9 shows the experimental set-up of a free jet issuing from a nozzle and the Michelson optics used. The nozzle exit diameter is d = 2 mm. The jet is produced by blowing carbon dioxide gas out of a pressure chamber into the atmosphere at ambient pressure. The tracer particles are condensed carbon dioxide particles.

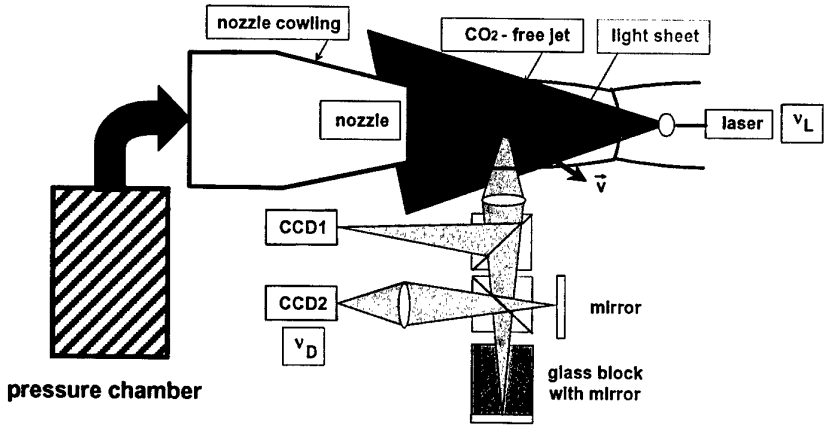

Fig. 9 Schematic of the nozzle flow and optical set up

The beam of a 1 W single-mode Ar^+-laser is transformed into a light sheet with a cross-section of 0.5 mm × 15 mm, passing axially through the longitudinal axis of the jet. The angle between the interferometer and the flow direction is adjusted to 90°. A glass block with a length of 180 mm and a refractive index of n = 1.52 is used. Figure 10a represents a Doppler picture of the jet taken with the CCD2 camera at a pressure in the pressure chamber of p ≈ 20 bar. The unshifted reference fringe system outside of the jet is simultaneously seen in Figure 10b. The light intensity picture in Figure 11, taken by the camera CCD1, shows the Mach disc generated downstream by underexpansion. Unfortunately, due to the shock strength, the temperature increases and the condensed carbon dioxide particles evaporate in a small region behind the shock wave. Figure 12 shows the Doppler picture (Figure 10a), normalized according to Equation (2) with the intensity I_0 image (Figure 11).

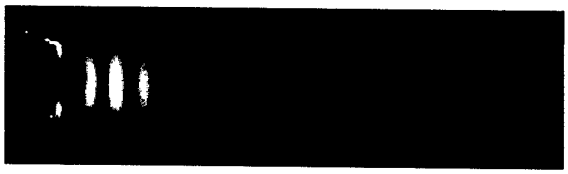

Fig. 10a Free jet Doppler picture from CCD2 camera

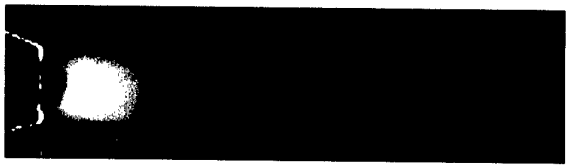

Fig. 11 Light intensity picture taken from CCD1 camera

Fig. 12 Normalized Doppler picture shown in pseudo colors

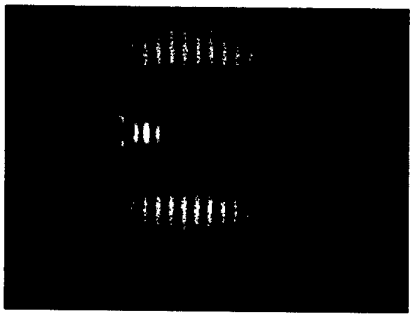

Fig. 10b Doppler picture of the jet with reference fringe distribution outside

In order to determine the velocities (Figure 13), the technique described in section 3.1 based on the pixel by pixel gray value evaluation is carried out by applying Equations (8) – (12). Two regions had been evaluated: a) shortly after the nozzle exit and b) downstream the recompression shock. The velocities determined by applying

Equations (12a, b) and Equation (1) along the center line of the left hand side region a) show some differences which are of the order of less than 5% compared to the one-dimensional theory, see Figure 14. The calculations give a higher expansion than the Doppler picture evaluation. In the calculation scheme some uncertainties are included, e.g., as its application to the three dimensional jet formation as well as the not exactly known pressure inside of the pressure chamber, so that the deviation between theory and the velocity distribution taken from the Doppler picture is acceptable. Moreover, the Doppler picture shows the formation of the radial structure of the jet in the domains evaluated and visualized in Figure 13. This outcomes support the good applicability of the DPV technique for planar flow velocity determination and visualization.

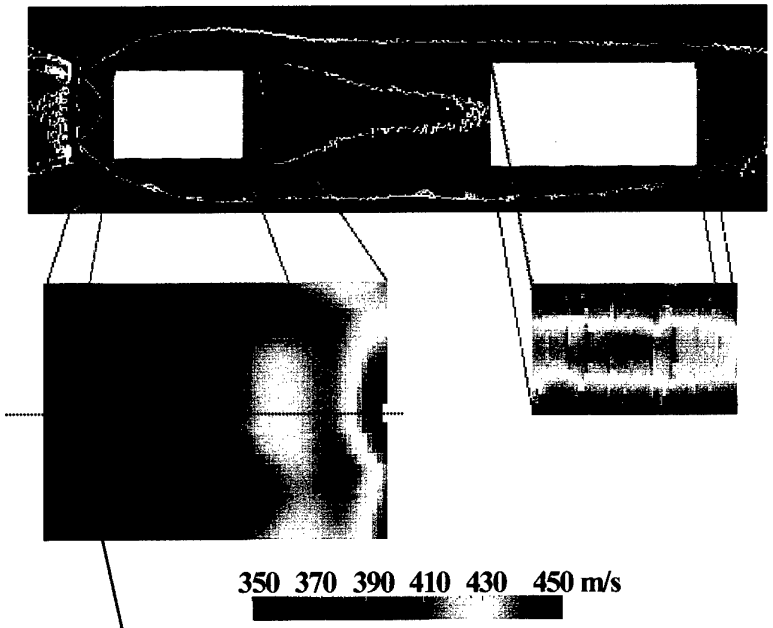

Fig. 13 Velocity distributions in pseudo colors

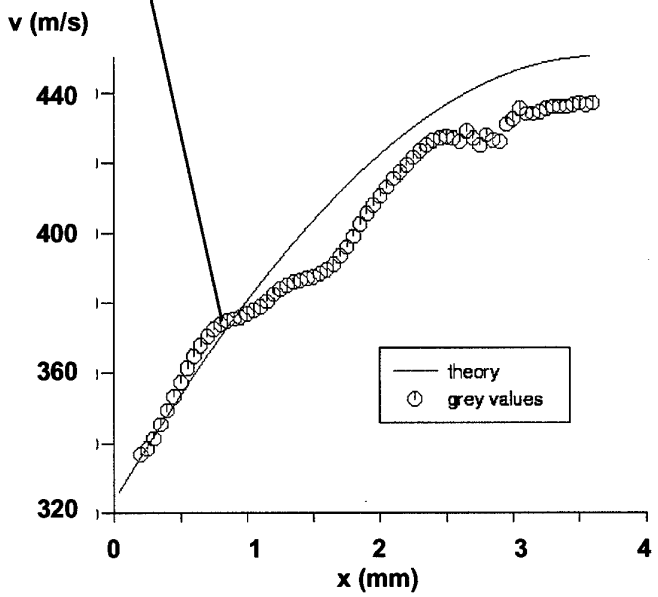

Fig. 14 velocity distribution along the jet center line

4. High speed wedge flow visualization

4.1 Description of shock tunnel facility

The DPV technique was applied to measure the vertical velocity component over a wedge in supersonic high speed flow. That flow is generated in the ISL/STB shock tunnel facility equipped with a conical nozzle used in direct mode and producing a Mach number 4.0 nitrogen flow out of the nozzle exit. Shortly after the nozzle exit, 50 mm downstream, a 15° wedge is placed slightly off axis (+7 mm) into the supersonic nozzle flow producing an attached oblique shock wave over the wedge surface. That shock wave turns the incoming flow parallel to the wedge surface. A principle sketch of the shock tunnel facility ISL/STB in which these experiments have been carried out is given in Figure 15. The shock tunnel consists of three parts: the high pressure driver section with driver pressure p_5, the driven section containing the test gas initially under pressure p_1, and the nozzle attached at the end of the driven tube. As driver gas hydrogen is used under a pressure of about $p_5 \approx 130$ bars. The driven tube nitrogen fill pressure was $p_1 = 2{,}2$ bars. After the burst of the diaphragm a shock wave is formed by which the test gas flow is initiated in the driven section and expanded via the shock tunnel nozzle in order to form the wedge on flow.

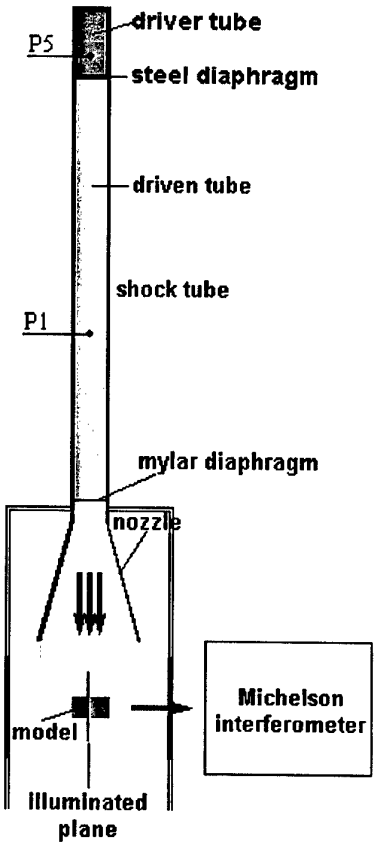

Fig. 15 Shock tunnel ISL/STB with measuring chamber

The wedge is mounted inside a dump tank which is equipped with windows at both sides and at the top. A light sheet is produced from top by a Neodym/YAG laser pulse (523 nm), see vector $\vec{e}_L$ in Figure 16, which illuminates a plane axially oriented in the middle of the wedge flow. The observation by the Michelson interferometer was done from the side, $\vec{e}_D$, and the flow vector $\vec{v}$ is directed vertically.

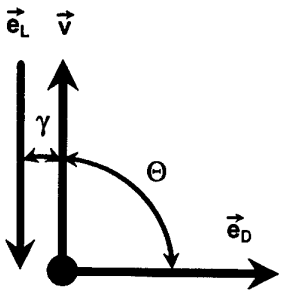

Fig. 16 Vector diagram

Figure 17 gives a view of the ISL shock tube laboratory. The shock tube used for the experiments reported herein is that on the right hand side, STB, and is operated as a shock tunnel in non-reflected mode. On the left hand, shock tube STA is located. The conical nozzle used at STB opens into the dump tank, see Figure 18, with the wedge mounted in front of the nozzle.

Fig. 17 Shock tube laboratory

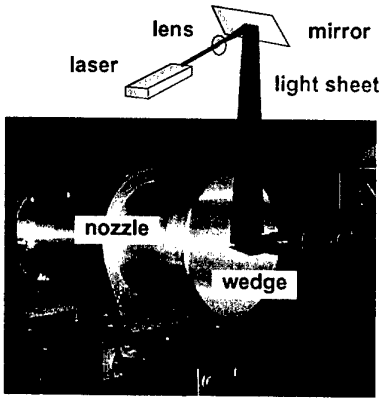

Fig. 18 Shock tunnel nozzle, wedge arrangement and illumination

4.2 Wedge flow visualization by DPV

In Figure 19 the initially adjusted fringe pattern present before flow onset can be seen in the light sheet plane formed over the wedge. In order to scatter the light coming from the top into the Michelson interferometer in case of no flow (no tracers), a diffuser plate was placed over the wedge surface. The interference fringe adjustment in turning mirror S_1 is clearly visible. The fringes appear slightly curved due to optics inaccuracies.

Because of the characteristics of the conical nozzle used for the experiments, the flow around the wedge is slightly divergent resulting in a vertical flow component, superimposed to the axial nozzle flow, which is in the range of maximum 5% of the axial velocity. Therefore, the fringe pattern in front of the oblique wedge shock wave is Doppler shifted as well as behind it in the region over the wedge surface. The fringe pattern as it looks for the wedge flow is given in Figure 20 (CCD2 camera). The wedge shock wave is clearly visible on the Doppler picture by means of a fringe shift caused by the velocity jump across the shock wave attached to the tip of the wedge. Over the wedge the flow turns vertically by flow deflection. That vertical velocity causes a Doppler shift of the frequency of the light scattered by tracer particles, here titanium dioxide (TiO_2) which results in a light intensity change across the wedge shock wave that appears as approximately one half fringe displacement in Figure 20. The processed flow region is marked in Figures 20 and 21 by a rectangle.

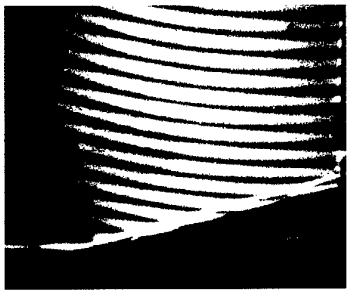

Fig. 19: Doppler picture taken before flow onset

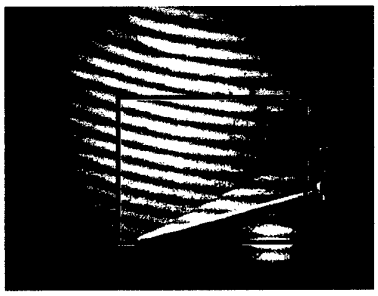

Fig. 20 Doppler picture in Σ'

As already seen in section 3.2, in gas flows the tracer particles are commonly not distributed homogeneously resulting in a distortion of the Doppler picture light intensity distribution I in the image plane Σ'. In order to solve this problem independently of light intensity fluctuations which influence the amplitude I_0 in Equation (2), a picture of the light intensity I_0 distribution, see Figure 21, is taken simultaneously with the Doppler picture. The optical set-up used is that in Figure 5. In dividing the two pictures pixel-wise, the Doppler picture light intensity distribution I (Figure 20) by the intensity picture I_0 of Figure 21, a normalized, I_0-independent Doppler picture results according to Equation (2) with $0 \le I/I_0 \le 1$. This intensity normalizing procedure must also be done for the Doppler picture taken initially before flow onset (Figure 19).

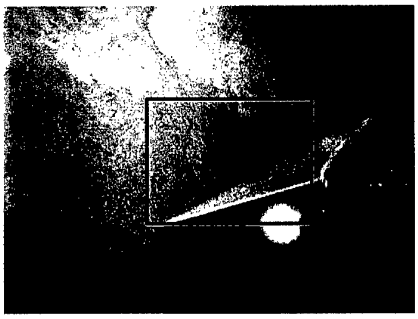

Fig. 21: Light intensity picture in Σ' on the CCD1 camera

At each pixel of the CCD2 camera (optical set-up see Figure 5), used for taking the Doppler and reference picture the light intensity is stored and the procedure explained in section 3.1, Equations (8) and (9), is applied.

Then, for calculating the phase difference $\Delta\varphi$, on the one hand before flow onset, $\Delta\varphi_L$, and on the other hand $\Delta\varphi_D$, given by Doppler shifted scattered light, Equations (10) and (11) are used. By subtracting both phase differences from each other, Equation (12b), the frequency shift $dv_L = v_D - v_L$ is obtained by applying Equation (12a). For calculating the amount of the tracer velocity $\vec{v}$ visualized with the Doppler picture in Figure 20, the relation deduced from Equation (1),

$$v = \frac{dv_L}{v_L} \frac{c}{2} \frac{1}{\cos\gamma \cdot \sin\theta/2} \quad , \tag{13}$$

is applied pixel by pixel.

4.3 DPV Velocity picture

The image processing software developed at ISL applies pixel-wise the procedure described in section 3.1. Thereby the distribution of the velocity $\vec{v}$ appearing in the light sheet plane was determined. The result is given in Figure 22 by means of the velocity picture which shows in pseudo colours the visualized formation of the vertical v-velocity component present in the nozzle flow in front of the oblique wedge shock wave and behind it over the surface of the wedge.

Looking at the velocity evaluation in Figure 22, deduced from the Doppler picture in Figure 20, the relative velocity changes Δv are given. Relative to zero velocity ($v = 0$) before flow onset, the vertical nozzle flow velocity is determined to $\Delta v = 100$ m/s. The measuring error is in the range of about 10%, i.e., $\pm$ 10 m/s. That flow region appears in Figure 22 in green colour. Across the wedge oblique shock wave, the measured velocity jump is of the order of $\Delta v = 260$ m/s $\pm$ 26 m/s, as visualized in the velocity picture of Figure 22 by a red coloured region and is constant between shock wave and wedge surface.

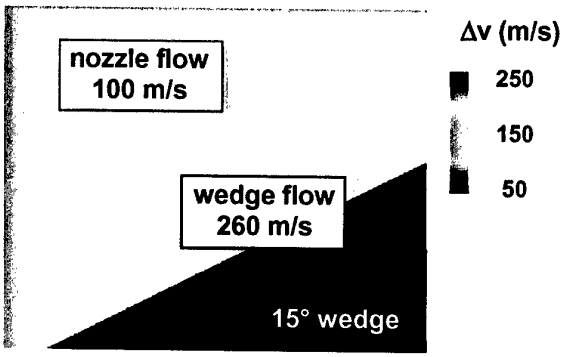

Fig. 22 Doppler picture visualized velocity changes in pseudo colours

4.4 Determination of nozzle flow

According to Equation (10), the reference fringe pattern in Figure 19 gives information on the phase difference distribution $\Delta\varphi_L$ before flow onset. Unfortunately, probably due to vibrations present during the experimental run, the reference fringe system in Figure 19 was found to be unstable. The reason is that some optical parts, especially the mirrors, are displaced resulting in a shift of the optical path length difference $\Delta\phi$, see Equation (3). This shift is much smaller than one fringe, but gives a uncertainty in the Doppler picture evaluation by applying Equation (12b) concerning the phase difference $\Delta\varphi_L$. It was found that the $\Delta\varphi_L$ deviation is of the order of one quarter of a fringe, so that the reference picture in Figure 19 cannot be used to correctly determine the absolute v-velocities in front of the oblique wedge shock wave and behind, only the relative ones. To obtain reliable information on the inexactness of the DPV determined flow velocity, another velocimetry system was applied, the so called Particle Image Velocimetry (PIV). Figure 23 shows the PIV-image for the u-velocity distribution in horizontal direction and Figure 24 that for the vertical v-speed. A detailed description of the application of the PIV method to shock tube high speed flows is given by Havermann et al. (2001).

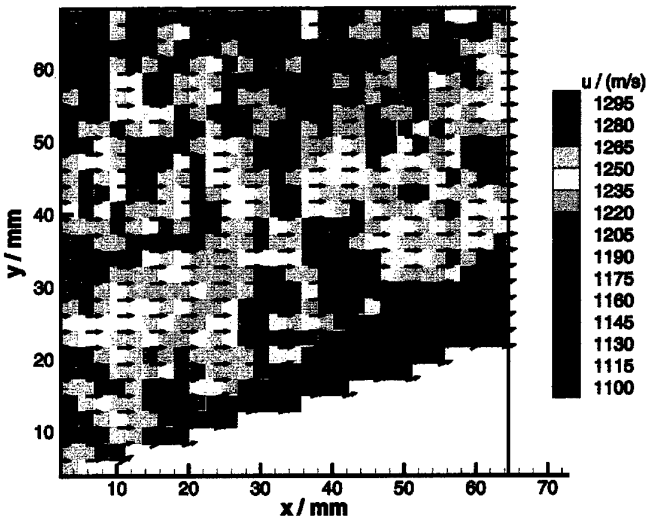

Fig. 23 Horizontal velocity distribution measured with PIV

In Figures 23 and 24 the 15° wedge ramp is located in the lower part of the diagram, seen in white colour. The velocity distribution which forms in the light sheet plane over the wedge is well established and is shown in terms of pseudo colours. The location of the oblique shock wave in front of the wedge surface can be determined as a strong velocity jump in both pictures, in the u-velocity of Figure 23 as well as the v-velocity in Figure 24. From Figure 23 the longitudinal u-velocity is determined in front and behind the oblique shock wave. Both values are deduced as mean samples coming from the interrogation regions used for PIV data reduction. Just as done for the axial u-velocity, also for the vertical v-velocity the data are deduced for the onflow and for the flow over the wedge surface. The following data are obtained:

front (green/red colours): u = 1257 ± 36 m/s, behind (blue colours): u = 1135 ± 33 m/s,

front (blue colours): v = 35 ± 22 m/s, behind (yellow/red colours): v = 305 ± 48 m/s.

In theory, by a solution of the conservation equations it follows that the shock wave influenced wedge flow is constant. Experimentally this prediction is confirmed by DPV as well as the PIV measurements, see Figures 22, 23 and 24. Moreover, the theoretical prediction gives v = 296 m/s which agrees well with the PIV measurement (v = 305 ± 48 m/s). In applying ISL's shock tube flow calculation procedures, the flow at the exit of the nozzle can be determined using the experimentally obtained data. From these deductions the wedge on flow is characterized as:

u = 1257 m/s, v = 35 m/s, M = 4.0, p = 42 kPa, T = 240 K.

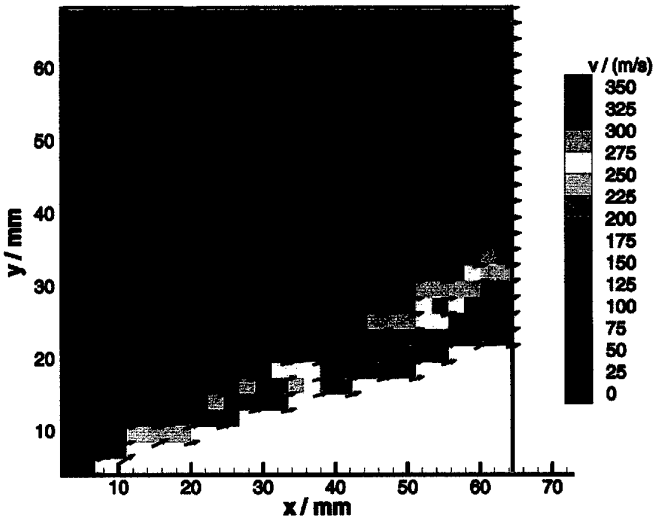

Fig. 24 Vertical velocity distribution measured with PIV

4.5 DPV reference picture calibration

As discussed in section 4.4, the PIV velocity visualization in Figure 23 shows that the wedge onflow produced by the conical shock tunnel nozzle flow is superimposed by a vertical velocity component of v = 35 ± 22 m/s. Looking at the velocity evaluation in Figure 22 deduced from the Doppler picture in Figure 20, there the vertical nozzle flow velocity was determined to v = 100 ± 10 m/s. This outcome does not agree with the v-velocity, v = 35 m/s, measured with the PIV technology which is successfully tested by Havermann et al (2001). The reason for the differences in the Doppler picture evaluation is already discussed in section 4.4 as a result of optical length $\Delta\phi$ variations between taking the reference Doppler picture (Figure 19) and Doppler picture (Figure 20), due to small vibrations of the optical parts inside the Michelson interferometer. In consequence, a systematic error develops which must be taken into account as a corrective speed factor. For the experiment described in section 4.2, that factor results to 65 m/s. In subtracting this corrective factor from the velocity data given in Figure 22, the absolute velocity distribution can be obtained as shown in Figure 25.

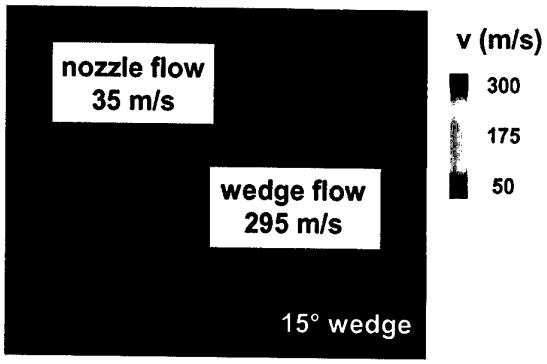

Fig. 25 Calibrated DPV velocity picture in terms of pseudo colours

If the reference interference picture is taken simultaneously with the Doppler picture, as done in the experiments described in sections 3.1 and 3.2, the absolute velocity distribution is available with a measuring error of about 10%. Due to mechanical instabilities, in case the reference picture is taken before taking the Doppler picture with the optical set-up shown in Figure 5, only velocity variations are given correctly, as the velocity jump across the wedge shock wave in the experiment carried out in the ISL shock tunnel STB. This jump is measured to $\Delta v = 260 \pm 26$ m/s. The PIV data in Figure 24 give: $\Delta v = 270 \pm 35$ m/s. This outcome suggests that the DPV technique at moment is only able to measure correctly velocity changes (e.g. the jump across the oblique wedge shock), because the reference and Doppler pictures are not simultaneously available.

5. Conclusions

The Doppler Picture Velocimetry (DPV) technique began in 1981 with the visualization of fringe shifts showing changes of flow velocity. At that time the fringe shift determination only gave information on the velocity changes in the flow area considered. Nowadays, in the enhanced DPV technique, the Doppler picture is taken with a CCD-camera and the output is treated pixel-wise using an appropriate software which is under development at ISL. The DPV concept, using the gray values, is a very powerful tool allowing to obtain information at any pixel of the plane crossing the flow.

To overcome the uncertainties concerning the reference picture which is taken before flow onset and discussed in section 4.2, a new Michelson system is established for taking the Doppler picture (phase difference $\Delta\varphi_D$) and the reference picture (phase difference $\Delta\varphi_L$) simultaneously. For that purpose, the optical set-up given in Figure 26, is under development and will be tested in future applications of flow velocity measurements in the ISL shock tunnel facilities. The new DPV tool uses three CCD cameras, CCD1 for taking the interference fringes resulting from the Doppler shifted frequency of the scattered light, CCD2 for taking the reference picture which uses unshifted laser light and CCD3 for taking the intensity distribution of the scattered light. The light passing the Michelson interferometer is polarized in order to separate the Doppler shifted light and the reference light which comes from a dispersion plate that is directly illuminated by the laser light source.

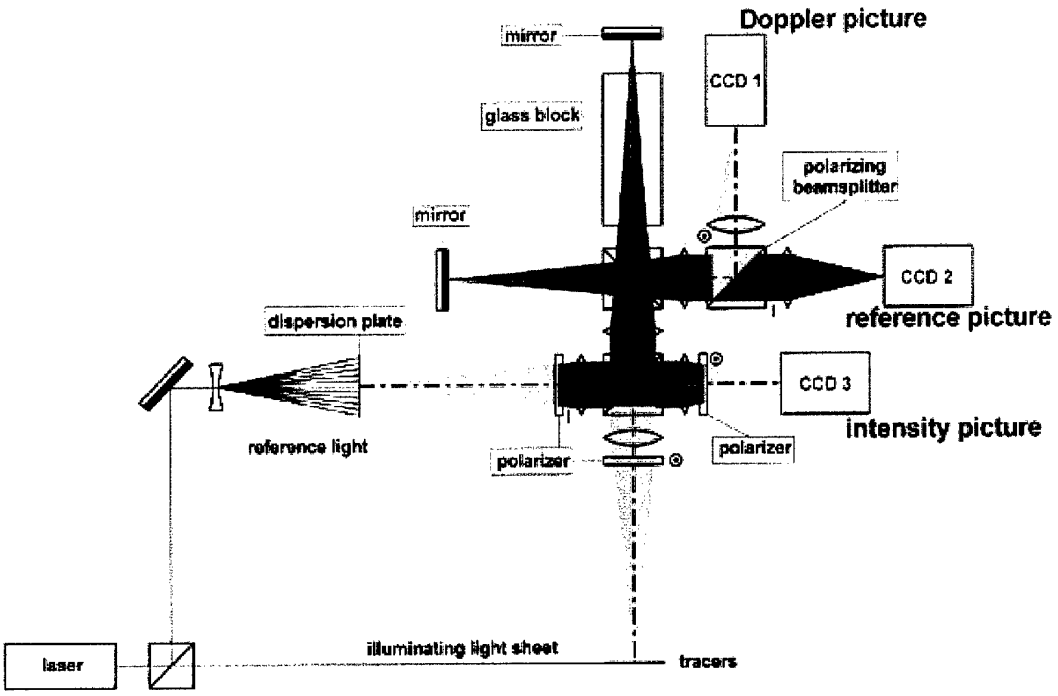

Fig. 26 Optical set-up for simultaneously taking Doppler (CCD1) and reference picture (CCD2)

6. References

Oertel H., Seiler F., George A., 1982, "Visualisierung von Geschwindigkeitsfeldern mit Dopplerbildern", ("Visualization of Velocity Fields with Doppler Pictures"), ISL-Report R 115/82

Seiler F., Oertel H., 1983, "Visualization of velocity fields with Doppler-pictures", 3rd International Symposium on Flow Visualization, Ann Arbor, Michigan, USA

Seiler F., George A., 1986, "Dopplerbilder von Freistrahlen", ("Doppler pictures of free jets"), ISL-Report N 602/86

Schneider A. L., 1987, "Konturverfolgung und Merkmalsgewinnung von Binärbildern mit Hilfe des RLC-Verfahrens", Diplomarbeit, Fachhochschule Ravenburg-Weingarten

Seiler F., Srulijes J., George A., 1987, "A Doppler-picture camera for velocity field visualization", 12th International Congress on Instrumentation in Aerospace Simulation Facilities, Williamsburg, VA, USA

Merzkirch W., 1990, "Laser -Speckle-Velocimetrie", In „Lasermethoden in der Strömungsmechanik", Hrsg. B, Ruck, AT-Fachverlag, Stuttgart

Seiler F., Srulijes J., George A., 1991, "Principles of laser Velocimetry with Doppler-pictures", SPIE's 36th Annual International Symposium on Optical and Optoelectronic Science and Engineering, San Diego, California, USA

Meyers J. F., 1992, "Doppler Global Velocimetry the next generation", AIAA 92-3897

Schumacher D., 1996, "Graphics", Gems III; pp.8, Oxford University Press

Seiler F., George A., Srulijes J, 1998, "Doppler Picture Interference Velocimetry (DPV)", 8th International Symposium on Flow Visualization, Sorrento, Italy

Seiler F., George A., Leopold F., Srulijes J., Smeets G., 1999, "Velocity Field Visualization Using Doppler Picture Interference Velocimetry", 18th International Congress on Instrumentation in Aerospace Simulation Facilities (ICIASF), Toulouse, France, ISL-Report PU 331/99

Leopold F., Seiler F., Schneider A., Srulijes J., Georges A., 2000, "Traitement des Images Doppler Interférentielles", 7ème Congrès Francophone de Vélocimétrie Laser, Marseille, France, ISL-Report PU 354/2000

Havermann M., Haertig J., Rey C., George A., 2001, "Particle Image Velocimetry (PIV) Applied to High Speed Shock Tunnel Flows", 23rd International Symposium on Shock Waves, Fort Worth, Tx, USA